Analytical and numerical investigation on the dynamic characteristics of entrapped air in a rapid filling pipe

Jiachun Liu, Jian Zhang and Xiaodong Yu

ABSTRACT

The entrapped air pockets in a pressurized water supply pipe may produce a significant transient pressure, resulting in pipe deformation or even pipe rupture. This article focuses on the maximum pressure of entrapped air pockets in a rapid filling pipe and its influencing factors. In this paper, the rigid water column theory and the ideal gas equation are applied to the air vessel-pressured pipe–air pocket system, and the theoretical formula representing the relationship between the maximum air pressure (MAP) and air comprehensive coefficient is presented. In addition, a numerical model of the system is established by the method of characteristics. The rapid filling process is simulated according to the experimental setup and the results are in good agreement with the experimental data. The influence of the air comprehensive coefficient on the MAP is also studied. Both the theoretical formula and numerical simulation show that the smaller air comprehensive coefficient will result in larger MAP (i.e., the MAP decreases with the increase of the polytropic exponent and initial air pressure, and increases with the increase of the initial air length).

Key words | air comprehensive coefficient, dynamic characteristics polytropic exponent, entrapped air pocket, maximum air pressure

Jiachun Liu
Jian Zhang
Xiaodong Yu (corresponding author)
College of Water Conservancy and Hydropower Engineering,
Hohai University,
Nanjing 210098,
China
E-mail: *yuxiaodong_851@hhu.edu.cn*

NOMENCLATURE

Symbols

Z_u Water level of upper steel air vessel
Z_t Top elevation of air chamber
P Pressure of the air pocket
P_u Air pressure in steel air vessel
γ Unit weight of water
z Absolute water level variation in air chamber
L Length of the diversion pipeline
m Polytropic exponent
Q Flow rate in the diversion pipe
α Total head loss coefficient in the diversion system
A Cross-sectional areas of the diversion pipe
F Cross-sectional areas of the air chamber
g Gravitational acceleration
l_0 Initial length of the air pocket
P_0 Initial absolute pressure of the air pocket
σ Air comprehensive coefficient
f Darcy–Weisbach friction factor
θ Angle of the pipeline inclined with the horizontal
x Distance along the pipeline
ξ Head loss coefficient of the spherical valve
z_c Stable water level variation in air chamber
z_m Maximum water level variation in air chamber

Acronym

MAP Maximum air pressure

doi: 10.2166/aqua.2018.153

INTRODUCTION

Air bubbles are easily entrapped in pipes forming air pockets in undulating water supply systems. If the pipeline system cannot discharge the air before the opening of the valve, the phenomenon of pressurized water flow-impacted entrapped air pockets in the pipeline system will inevitably appear. The pressure generated in this process is large and may cause damage to the pipeline system.

The prediction of pressure transient process in pipes with air is complicated, as it is related to air pocket size and movement, flow velocity and depth, pipe size and slope, venting and boundary conditions. The influence of entrapped air on abnormal transient pressures is often ambiguous because the compressibility of the air pocket permits the flow to accelerate but also partly cushions the system; the balance of these tendencies have been associated with the initial void fraction of the air pocket (Zhou *et al.* 2011). Compared with a single-phase water flow, free air increases the elasticity of the water and reduces the wave velocity, thus reducing the pressure pulsation during the transient process (Wylie *et al.* 1993). Experimental results show that an air pocket in pipeline system will produce a great pressure fluctuation in the hydraulic transient process (Vasconcelos & Wright 2011). For rapid filling scenarios, hydraulic bores, air–water interactions, and boundary reflections may lead to air pocket entrapment (Hamam & McCorquodale 1982; Li & McCorquodale 1999), which in turn can influence the transient pressure in the system because of compression, expansion, migration, and expulsion of the air pocket (Martin 1976; Aimable & Zech 2003; Zhou *et al.* 2011; Ferreri *et al.* 2014; Besharat *et al.* 2016). Many researchers have studied the rapid filling process in pipes with open ends, closed ends, orifice plates, or small air valves. Liou & Hunt (1996) analyzed the velocity variation of water in a rapid filling process, undulating, empty pipe with an open end. Zhou *et al.* (2002) presented experimental measurements from a horizontal pipeline in which the pipe length was constant and the inlet pressure was more than twice the atmospheric pressure; the work shows that when less air was present, the maximum pressure of the air pocket increased as the cushioning effect of the air pocket decreased. Chaudhry & Reddy (2011) analyzed the initial filling of an empty tunnel with a closed gate at the end and without an air vent before the gate. Zhou *et al.* (2011) carried out experiments to study pipes containing one or more air pockets and set up different ports for the tail of the pipe. Vasconcelos & Wright (2011) presented a model based on lumped inertia analysis which was developed by Lewis & Wright (2012). These models were successful in representing the experimental conditions presented by the authors, but failed in attempting to describe the severity of actual geysering episodes. Hou *et al.* (2013) investigated the filling velocity in rapid filling pipes with an open end. Martins *et al.* (2017) used a three-dimensional computational fluid dynamics model to simulate the rapid filling process and describe the maximum pressures of air pockets for a given range of initial conditions and compared the results with the experimental data. Muller *et al.* (2017) investigated air-related geysers that provide insight into the mechanisms of air release and the displacement of water in vertical shafts.

In a pipeline system with entrapped air pockets, the hydraulic transients between different conditions is complicated as the air pressure is a nonlinear restoring force, and the influencing factors on the maximum air pressure (MAP) and their relationship are unclear. Particularly, the analytical expression that addresses the effect of influencing factors on the MAP is not sufficient, which is more general than specific numerical simulation. In this paper, the rigid water column theory and the ideal gas equation are applied to the pipeline system, and the theoretical formula representing the relationship between the maximum pressure of air pocket and air comprehensive coefficient is deduced, thereby contributing to a more general understanding of the dynamic characteristics of entrapped air in a rapid filling pipe. In addition, the numerical model of the system is established based on the method of characteristics (Karney & Ghidaoui 1997; Miao *et al.* 2017; Liu *et al.* 2017), the rapid filling process is simulated based on the experimental setup and the results are compared with the experimental data. The influence of air comprehensive coefficient on the MAP is also studied. Numerical simulation of different operation conditions are carried out in order to clarify the

influence of the polytropic exponent, the initial air pressure and the initial air length on the MAP. Finally, the conclusions can provide a reference for the design and operation of water supply systems.

THEORETICAL ANALYSIS OF THE MAP AND ITS INFLUENCING FACTORS

Mathematical model

The ideal gas equation shows that as the length of the air pocket reaches its minimum value, the air pocket pressure is at maximum. Therefore, the investigation on the air pocket pressure can be transformed into the study of the variation of the length of the air pocket, then the air pocket pressure can be obtained by the ideal gas equation. Martins (2012) carried out physical experiments to study the dynamic characteristics of an entrapped air pocket. In this paper, the pipeline system is established based on a physical experiment setup (Martins *et al.* 2017), and the layout of the pipeline system is shown in Figure 1. Pipe 3, which contains an air pocket, can be treated as an air chamber. In the process of the theoretical analysis on MAP, the following assumptions are made: (a) ignoring the water inertia in the air chamber, (b) the water in the pipeline is incompressible, and (c) the friction in the pipeline is quasi steady.

The basic equations of the pipeline system with an entrapped air pocket are presented as follows (Chaudhry 2014).

Dynamic equation:

$$Z_u + \frac{P_u}{\gamma} - \left((Z_t - l) + \frac{P}{\gamma}\right) - \alpha|Q|Q = \frac{L}{gA}\frac{dQ}{dt} \tag{1}$$

Continuity equation:

$$Q = F\frac{dz}{dt} \tag{2}$$

Ideal gas equation:

$$Pl^{\mathrm{m}} = P(l_0 - z)^m = P_0 l_0^m \tag{3}$$

where Z_u is the water level of the upper steel air vessel. Z_t is the top elevation of the air chamber. P and P_u are the pressure of the air pocket and the air pressure in the steel air vessel, respectively. γ is the unit weight of water. l is the instantaneous equivalent air pocket length obtained by $l = l_0\text{-}z$, in which z is the absolute water level variation in the air chamber, measured positive upwards. L is the length of the pipeline. Q is the discharge in the pipeline. α is the total head loss coefficient in the diversion system, which is a constant during the transient process. F and A are the cross-sectional areas of the air chamber and diversion pipes, respectively. P_0 and l_0 are the initial absolute pressure and the length of the air pocket before the valve opens. m is the polytropic exponent, taken as 1.0 in the isothermal process and 1.4 in the adiabatic process. g is the acceleration due to gravity. t is time. Subscript 0 refers to the initial steady value.

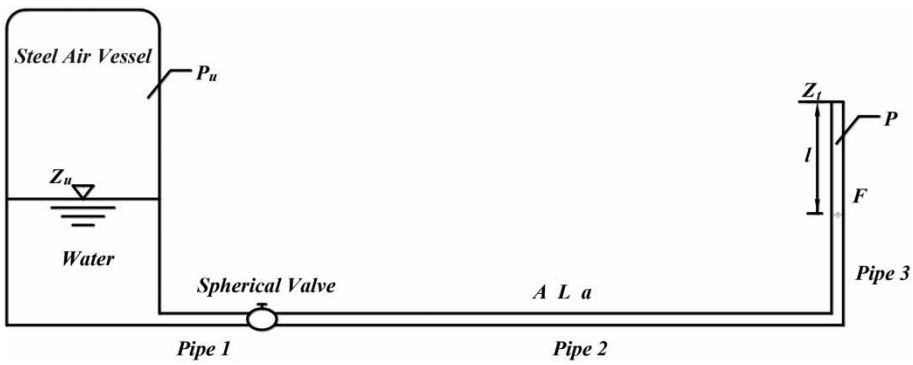

Figure 1 | Schematic diagram of pipeline system layout.

Using the first-order Taylor expansion, Equation (3) is deduced as:

$$P = P_0 \frac{l_0^m}{(l_0 - z)^m} \approx P_0\left(1 + \frac{mz}{l_0}\right) \tag{4}$$

Taking Equation (4) into Equation (1) results in:

$$z\sigma = \mu - \alpha|Q|Q - \frac{L}{gA}\frac{dQ}{dt} \tag{5}$$

where σ is defined as the air comprehensive coefficient, $\sigma = 1 + mP_0/\gamma l_0$, and $\mu = Z_u + P_u/\gamma\text{-}Z_t + l_0 - P_0/\gamma$. As the pressure on the left side of the spherical valve is greater than the right side as the valve is closed, the value of μ is greater than zero.

Formula derivation

Solving Equations (2) and (5) by eliminating dt results in:

$$z\sigma = \mu - \alpha|Q|Q - \frac{L}{2gAF}\frac{dQ^2}{dz} \tag{6}$$

Since the highest water level appears at the end of water flows into the air chamber, the value of flow rate in pipes is positive during the transition process, so the absolute value sign can be removed. Therefore, Equation (6) can be simplified as:

$$\frac{dQ^2}{dz} = \varphi\mu - \varphi\alpha Q^2 - \varphi\sigma z \tag{7}$$

where $\varphi = 2gAF/L$, φ is the constant greater than zero.

Then, the integral solution of Equation (7) is obtained by using a variation of parameters method, resulting in:

$$Q^2 = \frac{\mu - \sigma z}{\alpha} + \frac{\sigma}{\varphi\alpha^2} + C_1 e^{-\varphi\alpha z} \tag{8}$$

where C_1 is an integral constant.

When the system reaches a new steady state, the flow rate in the pipe becomes zero and the water level variation in the chamber becomes z_c, where z_c is the absolute value between the new steady water level and the initial chamber water level, and the actual value of z_c is positive. Taking $Q = 0$, $z = z_c$ into Equation (8) gives:

$$C_1 = -\frac{\sigma}{\varphi\alpha^2} e^{\varphi\alpha z_c} \tag{9}$$

Therefore, the final solution of Equation (7) is:

$$Q^2 = \frac{\mu - \sigma z}{\alpha} + \frac{\sigma}{\varphi\alpha^2}\left(1 - e^{\varphi\alpha(z_c - z)}\right) \tag{10}$$

when the discharge in the pipe equals zero, the water level in the air chamber reaches the maximum value (i.e., $Q = 0$, $z = z_m$), where z_m is the absolute value between the maximum water level and the initial chamber water level, and the actual value of z_m is positive. Taking $Q = 0$, $z = z_m$ into Equation (10) gives:

$$\sigma = \frac{\varphi\alpha\mu}{(\varphi\alpha z_m - 1 + e^{\varphi\alpha(z_c - z_m)})} \tag{11}$$

when the system reaches a new steady state, the discharge in the pipe becomes zero and the water level variation in the air chamber becomes z_c. Taking $Q = 0$, $z = z_c$ into Equation (5) can draw $z_c = \mu/\sigma$, then Equation (11) can be simplified to:

$$\varphi\alpha z_m - 1 + e^{\varphi\alpha\left(\frac{\mu}{\sigma} - z_m\right)} = \frac{\varphi\alpha\mu}{\sigma} \tag{12}$$

Define $\varepsilon = \varphi\alpha\mu/\sigma$, then Equation (12) can be simplified to:

$$\varphi\alpha z_m - 1 + e^{\varepsilon - \varphi\alpha z_m} = \varepsilon \tag{13}$$

Taking derivatives of ε on both sides of Equation (13) gives:

$$\varphi\alpha\frac{dz_m}{d\varepsilon}(1 - e^{\varepsilon - \varphi\alpha z_m}) = (1 - e^{\varepsilon - \varphi\alpha z_m}) \tag{14}$$

when the system reaches a new steady state, the water level variation in the air chamber will be less than the maximum

water level variation (i.e., $z_c - z_m < 0$), therefore $1 - e^{-\varphi\alpha z m} \neq 0$. The following formula is available:

$$\frac{dz_m}{d\varepsilon} = \frac{1}{\varphi\alpha} > 0 \tag{15}$$

Simplifying Equation (3) yields $z = (l_0/m)(P/P_0\text{-}1)$. Taking $z = (l_0/m)(P/P_0\text{-}1)$ and $\varepsilon = \varphi\alpha\mu/\sigma$ into Equation (15) gives:

$$\frac{dP_m}{d\sigma} = -\frac{\mu m P_0}{\sigma^2 l_0} < 0 \tag{16}$$

where P_m is the MAP.

As illustrated in Equation (16), the air comprehensive coefficient, a parameter reflecting the initial state of the air pocket in the system, has an important effect on the maximum pressure of the air pocket during the transient process. In the case of keeping other parameters constant, the increase of the air comprehensive coefficient will lead to the decrease of MAP. Thus, the smaller air comprehensive coefficient will result in a larger MAP. It can be seen from the ideal gas equation and the expression of the air comprehensive coefficient that when the initial water level in the air chamber and other parameters is constant, the increase of the polytropic exponent and the initial air pressure will lead to the increase of the air comprehensive coefficient, resulting in a decrease in the MAP. The air comprehensive coefficient decreases with the increase of the initial air pocket length, leading to the increase of the MAP. Thus, keeping other parameters constant, larger initial air pocket length will result in a higher MAP.

NUMERICAL INVESTIGATION

Experimental model

An experiment was conducted by Martins *et al.* (2012) to study the maximum pressure of an air pocket in a pipeline system. The model layout diagram and the main parameters of the system are shown in Figure 1 and Table 1. The physical experimental rig mainly consists of the following parts: steel air vessel, water pipe, spherical valve, water pipe, closed end of vertical pipe with an air pocket. Pipes are made of polyvinyl chloride (PVC), with an inner diameter of 0.0536 m and a wall thickness of 4.7 mm. The spherical valve links the pressure steel air vessel and the water pipes with an inner diameter of 0.0536 m and opened totally in 0.23 s.

Table 1 | Main parameters of the experimental rig

Pipe	Length/m	Diameter/m	Steel air vessel	
1	0.24	0.0536	Diameter/m	0.80
2	2.00	0.0536	Volume/m^3	1.00
3	1.38	0.0536	Water Volume/m^3	0.40

In the initial operating condition, the spherical valve is closed. The pressure on the left side of the valve is greater than the pressure on the right side, so there is a pressure difference between the two sides. When the valve is opened, the water flows from part A to part B through a vertical pipe. As the water level in part B rises, the air pocket is compressed and the air pocket pressure is increased. When the water level reaches the maximum in part B, the air pocket pressure reaches its maximum value as well. At this moment, the air pressure in part B is greater than the air pressure in the left steel air vessel. The water begins to flow in the opposite direction due to the pressure difference. Due to the presence of friction in the system, water level fluctuations are always diminishing, but the water level will reach a new stable state after a while. To understand the dynamical behaviors of the filling process and the water–air interaction, one-dimensional (1D) numerical simulation is conducted in the following sections.

1D method of characteristics model

Pressurized pipe model

The following equations are used to describe the transient flow in pipes (Wylie *et al.* 1993).

Continuity equation:

$$\frac{\partial H}{\partial t} + V\frac{\partial H}{\partial x} + \frac{a^2}{g}\frac{\partial V}{\partial x} + V\sin\theta = 0 \tag{17}$$

Momentum equation:

$$\frac{\partial H}{\partial x}+\frac{V}{g}\frac{\partial V}{\partial x}+\frac{1}{g}\frac{\partial V}{\partial t}+\frac{f|V|V}{2gD}=0 \tag{18}$$

where H is the piezometric head. V is the flow velocity. a is the wave speed. g is the acceleration due to gravity. f is the Darcy–Weisbach friction factor. θ is the angle of the pipeline inclined with the horizontal. x is the distance along the pipeline measured positive in the downstream direction. D is the diameter of the pipe. t is time.

The momentum and continuity equations governing transient flow in closed conduits are classified as hyperbolic partial differential equations for which no analytical solutions are available for a general pipe system. The method of characteristics is widely used to solve the set of partial differential equations. The method of characteristics is the most commonly used numerical method for solving hydraulic transient process in a pipeline system. The method of characteristics is a kind of approximate calculation method for solving the hyperbolic partial differential equation based on the characteristic theory of the partial differential equation (Wylie *et al.* 1993). If the problem is simple, the analytical solution or approximate analysis solution can be solved by this method. If the problem is complicated, a numerical solution of high accuracy can be obtained. The method of characteristics has many advantages: (1) stability criteria can be established; (2) boundary conditions are easy to program; (3) it is applicable to all kinds of pipeline hydraulic transient analysis; and (4) it has better precision than all the other different methods.

Spherical valve model

The mathematical model describing the characteristics of the spherical valve is:

$$H_{P1}-H_{P2}=\xi\frac{Q_P^2}{2gA_m^2} \tag{19}$$

where H_{P1} and H_{P2} are the piezometric heads at each side of the spherical valve, respectively. ξ is the head loss coefficient of the spherical valve. Q_P is the flow rate through the valve. A_m is the area of the valve. The head loss coefficient ξ under different valve opening τ is provided by the manufacturer, and the diameter of the spherical valve used in this paper is 0.0536 m. Substituting compatibility equations (Wylie *et al.* 1993) into Equation (19) results in:

$$Q_p=\frac{C_p-C_M}{B_p+B_M+\xi|Q_{p0}|/(2gA_m^2)} \tag{20}$$

in which the coefficients C_P, B_P, C_M, and B_M are constants, and Q_{P0} is the discharge of the previous time step. Q_P is the calculated discharge.

Mathematical model parameters

In this case, the method of characteristics is used to simulate the pipeline transition process with the closed air pocket under the condition of valve opening, and the results are compared with the experimental results. The layout of the numerical simulation system is the same as the experimental system, shown in Figure 1. The lengths of pipe 1, pipe 2, and pipe 3 are 0.24 m, 2.00 m, and 1.38 m, respectively. The diameter of all the pipes is 0.0536 m, and the pipe roughness is 0.012. The wave velocity of water in the pipeline is 450 m/s. The initial pressure of the air pocket is the atmospheric pressure (i.e., 10.33 m). The bottom elevation of the pipeline is 0.0 m. The spherical valve is closed under the initial condition and opens totally in 0.23 s with one-stage linear open law.

Comparison with experimental results

The selected conditions are that the initial pressure of the air in the steel air vessel is 20.66 m and the initial air pocket length in part B is different under different conditions. The polytropic exponent is taken as 1.4. The maximum air pocket pressure difference and air pocket pressure variation are shown in Figure 2 and Table 2. It can be seen that although the maximum pressure of the air pocket is different in both cases, the differences are smaller relative to the MAP obtained by the physical experiment. In addition, the pressure variations of the air pocket are in agreement with each other in different conditions. Therefore, the numerical results have certain accuracy and can satisfy the accuracy requirements of the following research.

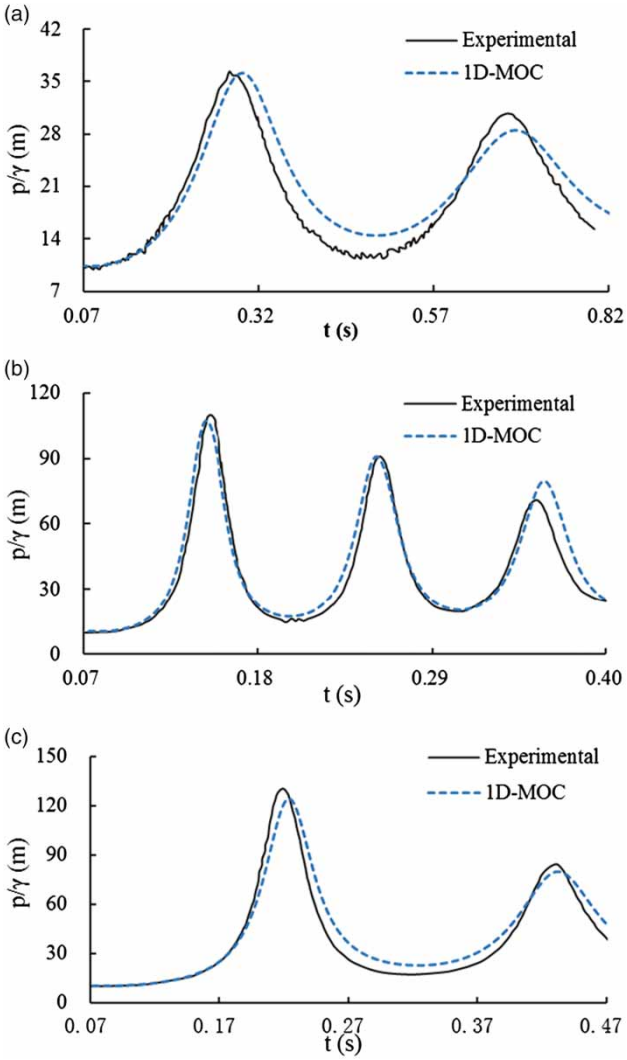

Figure 2 | Air pocket pressure comparison under three conditions: (a) condition *a* ($h_0 = 1$, $L_{air0}\backslash D = 9.3$); (b) condition *b* ($h_0 = 1$, $L_{air0}\backslash D = 1.9$); (c) condition *c* ($h_0 = 3$, $L_{air0}\backslash D = 9.3$).

Table 2 | Maximum air pocket pressure difference under three conditions

Condition	Maximum experiment pressure/m	Maximum simulation pressure/m	Pressure difference/m	Relative error/%
a	36.4	36.0	0.4	1.10
b	110.0	107.4	2.6	2.36
c	130.6	124.5	6.1	4.67

Influencing factors on MAP

Under the guidance of the analytical expression between the air comprehensive coefficient and the maximum pressure of air pocket, this section investigates the effects of initial air pressure, polytropic exponent, and initial air length on the maximum pressure of the air pocket by using a control variate method. It is generally believed that the process of air transition in the pipes is between the adiabatic process and the isothermal process (i.e., $m = 1.0 \sim 1.4$). Therefore, the polytropic exponents take m as 1.0, 1.2 and 1.4 for comparison, respectively. The initial air pocket pressure is 10.33 m and the initial air length is 0.102 m. The calculated results are shown in Figure 3.

As shown in Figure 3, with the other parameters remaining unchanged, the maximum air pocket pressure is decreasing with the increase of the polytropic exponent. The smaller polytropic exponent resulted in the larger MAP. When the polytropic exponent is taken as 1.4, the difference between the calculated maximum pressure of the air pocket and the experimental results is small. With the decrease of the polytropic exponent, the difference between the experimental results and the numerical results began to increase. When the polytropic exponent is taken as 1.0, the numerical simulation result of MAP is 125.02 m, which is 15.00 m higher than the experimental data. The polytropic exponent is an uncertain factor in the experiment, and the value of polytropic exponent in each experiment may not be the same due to the experimental instrument and the experimental environment. The MAP decreases with the increase of the polytropic exponent, which agrees with the theoretical analysis.

It can be seen from the theoretical analysis (Equation (16)) that the increase of the initial air pressure will change the value of the air comprehensive coefficient, affecting the MAP during the transient process. To verify this conclusion, the rapid filling process with different initial air pressure is simulated, and the effects of initial air

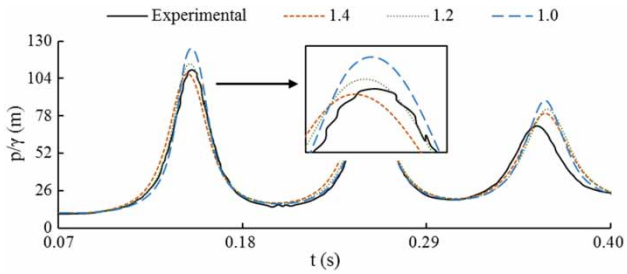

Figure 3 | Air pocket pressure versus time under different polytropic exponents.

pressure on maximum pressure of the air pocket are also analyzed. In this simulation, the polytropic exponent is taken as 1.4, the initial air length is taken as 0.102 m, and the initial water level in the air chamber is taken as the same value under different conditions. The initial air pressures are 10.33, 12.33, 14.33, and 16.33 m, respectively, and the corresponding calculation results are shown in Table 3 and Figure 4.

It can be seen from Table 3 and Figure 4 that with the increase of the initial air pressure, the air comprehensive coefficient also increased, and the maximum water level and the MAP are decreasing as the initial water level remains the same. The results are consistent with the theoretical analysis, which shows that the maximum pressure of the air pocket decreases as the initial air pressure increases when the other parameters are kept constant.

As discussed in the previous section, the MAP increases with the increase of initial air pocket length. Experimental results conducted by Martins *et al.* (2017) proved this conclusion. In the experimental study of Martins *et al.* (2017), the initial air pocket length was chosen to be 1.9 times and 9.3 times the diameter of the vertical pipe, respectively, and other parameters were kept constant. L_{air0} is the initial air pocket length and D is the diameter of the vertical pipe. The experimental results are shown in Figure 5.

It can be seen from Figure 5 that the larger initial air pocket length results in the larger MAP. When the initial air pocket length was chosen to be 1.9 times the diameter of the vertical pipe, the MAP appeared at 0.15 s, and the value of MAP was 109.99 m. When the initial air length was chosen to be 9.3 times the diameter of the vertical pipe, the MAP appeared at 0.22 s, and the value of MAP was 130.59 m. The MAP increases with the increasing initial air pocket length, which verified the theoretical analysis.

The influence of the different air pocket volumes on the MAP has been verified by the experimental model, by which the initial air length influenced the MAP indirectly. However, the volume of the air pocket is constant in some real cases, and the effect of the shape parameters on the MAP is not understood. As the MAP increases with the increasing initial air length, it is possible to reduce the MAP by reducing the length of the initial air pocket. The diameter of the air pocket will increase as the length of the air pocket decreases when the initial volume of the air pocket is constant. Therefore, the purpose of this section is to study the effect of different diameters of air pocket on the MAP with the constant initial volume and initial pressure of entrapped air pocket. The polytropic exponent is taken as 1.4, the initial air pressure is taken as 10.33 m, the diameter of the pipes are taken as 0.038, 0.054, and 0.121 m and the initial air length are taken as 1.00, 0.50, and 0.10 m, respectively. The initial parameters and corresponding results are shown in Figure 6.

As shown in Figure 6, when the initial volume and initial pressure of the air pocket are constant, the initial air length increases as the diameter of the air pocket decreases, resulting in the increase of the MAP. When the initial air length is 0.10 m, the MAP is 107.40 m and the maximum water level

Table 3 | Calculation results under different initial air pressure

Initial air pressure/m	Air comprehensive coefficient	Initial water level/m	Highest water level/m	MAP/m
10.33	142.78	1.278	1.361	107.40
12.33	170.24		1.357	103.40
14.33	197.69		1.354	100.89
16.33	225.14		1.352	99.22

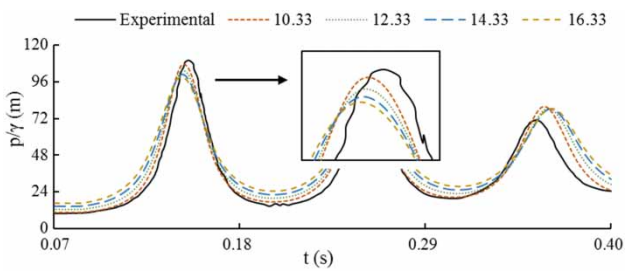

Figure 4 | Air pocket pressure versus time with different initial air pressure.

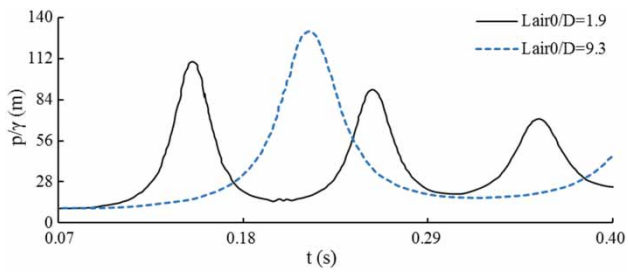

Figure 5 | Air pocket pressure versus time with different initial air pocket length.

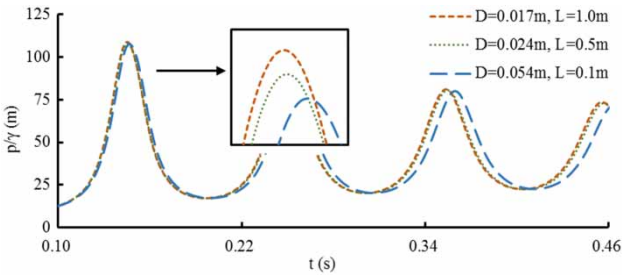

Figure 6 | Air pocket pressure versus time with different diameter and length of air pocket.

variation is 0.083 m. When the initial air length is 1.00 m, the MAP is 108.87 m and the maximum water level variation is 0.814 m. As the numerical model parameters in this case are relatively small, the MAP difference is not significant, while the change law of the MAP with the increase of the initial air length is confirmed. The experimental data and numerical simulation results verified the theoretical derivation. In addition, the numerical results illustrate that the MAP decreases with the increase of the diameter of the pipe containing the entrapped air when the initial volume of the air pocket is constant.

CONCLUSIONS

The entrapped air pockets in a pressurized water supply pipe may produce a significant transient pressure, resulting in pipe deformation or even pipe rupture. In this paper, the mathematical model of the air vessel-pressured pipe–air pocket system based on the rigid water column theory and the ideal gas equation is established, and the theoretical formula reflecting the relationship between the MAP and air comprehensive coefficient is presented. In addition, the numerical model of the system is established based on the method of characteristics. The rapid filling process of a pipeline system is simulated based on the experimental setup, and the results have been compared with the experimental data collected by Martins *et al.* (2017). A good agreement compared with the experimental data proved that the numerical model of the system has good precision. The influence of air comprehensive coefficient on the maximum pressure of the air pocket is studied, and both the theoretical formula and numerical simulation showed that the air comprehensive coefficient has a great influence on the maximum pressure of air pocket. This study found that the maximum pressure of entrapped air pocket and the fluctuation of water level in the air chamber will decrease with the increase of the air comprehensive coefficient during the rapid filling process. Air comprehensive coefficient reflects the initial characteristics of the entrapped air pocket, whose value is related to polytropic exponent, initial air pressure, and initial air length. With the increase of polytropic exponent and initial air pressure, the MAP is decreased; when the initial volume and initial pressure of the air pocket are constant, when the initial air length increased, the diameter of the air pocket decreased, resulting in the increase of the MAP.

Currently, some of the dynamic characteristics of the entrapped air pocket are understood theoretically, but more in-depth research needs to be carried out to translate these laws into effective mitigation methods.

ACKNOWLEDGEMENTS

This paper was supported by the National Key Research and Development Program of China (Grant No. 2016YFC0401810) and the Fundamental Research Funds for the Central Universities (Grant Nos 2016B10814, 2016B41714 and 2016B04914).

REFERENCES

Aimable, R. & Zech, Y. 2003 Experimental results on transient and intermittent flows in a sewer pipe model. *Proceedings of the 30th IAHR Congress*, Vol. B, Thessaloniki, Greece, pp. 377–384.

Besharat, M., Tarinejad, R. & Ramos, H. M. 2016 The effect of water hammer on a confined air pocket towards flow energy storage system. *Journal of Water Supply: Research and Technology-AQUA* **65** (2), 116–126.

Chaudhry, M. H. 2014 *Applied Hydraulic Transients*. Springer, New York, USA.

Chaudhry, M. H. & Reddy, H. P. 2011 Mathematical modeling of lake tap flows. *Journal of Hydraulic Engineering* **137** (5), 611–614.

Ferreri, G. B., Ciraolo, G. & Lo Re, C. 2014 Storm sewer pressurization transient–an experimental investigation. *Journal of Hydraulic Research* **52** (5), 666–675.

Hamam, M. & McCorquodale, J. 1982 Transient conditions in the transition from gravity to surcharged sewer flow. *Canadian Journal of Civil Engineering* **9** (2), 189–196.

Hou, Q., Tijsseling, A. S., Laanearu, J., Annus, I., Koppel, T., Bergant, A., Vučković, S., Anderson, A. & van't Westende, J. M. C. 2013 Experimental investigation on rapid filling of a large-scale pipeline. *Journal of Hydraulic Engineering* **140** (11), 04014053.

Karney, B. W. & Ghidaoui, M. S. 1997 Flexible discretization algorithm for fixed-grid MOC in pipelines. *Journal of Hydraulic Engineering* **123** (11), 1004–1011.

Lewis, J. W. & Wright, S. J. 2012 Air-water interactions that generate large water lift through vertical shafts in stormwater conduits. *Journal of Water Management Modeling* **2**, 21–44. doi:10.14796/JWMM.R245-02.

Li, J. & McCorquodale, A. 1999 Modeling mixed flow in storm sewers. *Journal of Hydraulic Engineering* **125** (11), 1170–1180.

Liou, C. P. & Hunt, W. A. 1996 Filling of pipelines with undulating elevation profiles. *Journal of Hydraulic Engineering* **122** (10), 534–539.

Liu, J. C., Zhang, J., Chen, S. & Yu, X. D. 2017 Investigation on maximum upsurge and air pressure of air cushion surge chamber in hydropower stations. *Journal of Pressure Vessel Technology-Transactions of the ASME* **139** (3), 031603.

Martin, C. S. 1976 Entrapped air in pipelines. *Proceedings of the 2nd International Conference on Pressure Surges*, British Hydromechanics Research Association, Bedford, UK, pp. 15–28.

Martins, S. C. 2012 *Pressurization Dynamics of Hydraulic Systems with Entrapped Air*. PhD thesis, Instituto Superior Técnico, Universidade de Lisboa (in Portuguese).

Martins, S. C., Martins, N. M. C., Ramos, H. M. & Almeida, A. B. 2012 Liquid flow and entrapped air behaviours in an experimental set-up using CFD analysis. *Proceedings of the 11th International Conference on 'Pressure Surges' – Surge Analysis*, Lisbon, Portugal, pp. 505–516.

Martins, N. M. C., Delgado, J. N., Ramos, H. M. & Covas, D. I. C. 2017 Maximum transient pressures in a rapidly filling pipeline with entrapped air using a CFD mode. *Journal of Hydraulic Research* **55** (4), 506–519.

Miao, D., Zhan, J., Chen, S. & Yu, X. D. 2017 Water hammer suppression for long distance water supply systems by combining the air vessel and valve. *Journal of Water Supply: Research and Technology-AQUA* **66** (5), 319–326.

Muller, K. Z., Wang, J. & Vasconcelos, J. G. 2017 Water displacement in shafts and geysering created by uncontrolled air pocket releases. *Journal of Hydraulic Engineering* **143** (10), 04017043.

Vasconcelos, J. G. & Wright, S. J. 2011 Geysering generated by large air pockets released through water-filled ventilation shafts. *Journal of Hydraulic Engineering* **137** (5), 543–555.

Wylie, E. B., Streeter, V. L. & Suo, L. S. 1993 *Fluid Transients in Systems*. Prentice Hall, New York, USA.

Zhou, F., Hicks, F. E. & Steffler, P. M. 2002 Transient flow in a rapidly filling horizontal pipe containing trapped air. *Journal of Hydraulic Engineering* **128** (6), 625–634.

Zhou, L., Liu, D. Y., Karney, B. & Zhang, Q. 2011 Influence of entrapped air pockets on hydraulic transients in water pipelines. *Journal of Hydraulic Engineering* **137** (12), 1686–1692.

First received 16 September 2017; accepted in revised form 14 December 2017. Available online 2 January 2018